Pixels with add-on structures to enhance quantum efficiency in the near infrared

Félix Bardonnet, Axel Crocherie, Marios Barlas, Quentin Abadie, Clémence Jamin

Pixels with add-on structures to enhance quantum efficiency in the near infrared

F. Bardonnet*[ab], A. Crocherie [a], M. Barlas [a], Q. Abadie [c], C. Jamin-Mornet [c]
[a]STMicroelectronics, 850 rue Jean Monnet, 38920 Crolles, France; [b]2 Univ. Paris-Saclay, Institut d'Optique Graduate School, CNRS, Laboratoire Charles Fabry, 91127, Palaiseau, France; [c]CEA LETI, 17 avenue des Martyrs, 38054 Grenoble, France ; *felix.bardonnet@st.com

ABSTRACT

Due to their low-cost fabrication process and high efficiency, silicon-based Complementary Metal Oxide Semiconductor (CMOS) image sensors are the reference in term of detection in the visible range. However, their optical performances are toughly degraded in the Near Infrared (NIR). For such wavelengths, Silicon has a small absorption coefficient, leading to a very poor Quantum Efficiency (QE). A solution to improve it is to implement structures like pyramids that are etched in the Silicon layer. This will lead to diffraction inside the photodiode, enhancing the light path and therefore the absorption. Using Finite Difference Time Domain (FDTD) simulations, we demonstrated a huge QE enhancement at 940nm on real pixels, by implementing this kind of diffractive structures and we finally confirmed these results by characterizations. We obtained QE values up to 47% at 940nm for our 3.2µm pixel, corresponding to a gain of 2 comparing to a pixel without any diffractive structures. We also measured the Modulation Transfer Function (MTF), to evaluate how this figure of merit is impacted by the addition of these structures. As expected, the MTF was degraded when we added these diffractive patterns but were still high looking at the values. We indeed demonstrated MTF values going up to 0.55 at Nyquist/2 frequency and 0.35 at Nyquist frequency. Looking not only at QE values but also at MTF ones, these are very promising results that could be used in many different NIR applications like face recognition, Light Detection and Ranging (LIDAR) or AR/VR.

Keywords: CMOS image sensors, Near infrared, Quantum efficiency, Modulation transfer function

1. INTRODUCTION

To answer to a need in numerous new applications like face recognition or LIDAR, where light cannot be visible to the human eye, new CMOS image sensors working in the NIR have emerged. The principal problem with these sensors is the weak absorption of Silicon in this wavelength range (850nm to 1100nm). This is linked to the intrinsic nature of the Silicon bandgap (indirect), that will imply a weak absorption near the bandgap energy (1.12eV), which corresponds to the energy of a photon with a 1100nm wavelength. The first thing that comes in mind is therefore to replace Silicon by low bandgap semiconductors. However, it usually comes with strong dark current, temporal noise increase, process integration compatibility issues to standard semiconductor fabs (with III-V materials), and significantly higher fabrication cost. Another solution would be to create a Fabry-Perot cavity inside the pixel. Light would therefore bounce back and forth several times in the photodiode, enhancing its light path inside, and thus increasing the absorption. We can see an example of such so-called Resonant Cavity Enhanced photodiode (RCE) [1], where the cavity is formed using a Distributed Bragg Reflector (DBR) on one side and the air-Silicon interface on the other side. The problem here would be a process dispersion problem. With such Fabry-Perot cavities, we indeed see narrow interference peaks at the resonant wavelengths, which are dependent on the cavity and Fabry-Perot layers thicknesses as well as on the wavelength of the incoming light and the incident angle of the light. Thus, in order to have the interference peak at the wavelength of interest (940nm for example), we would need to match the right thicknesses of the different layers which is already too difficult to achieve perfectly and reproduce it on every pixel. Moreover, depending on the position of the pixel on the sensor, light is not coming with the same angle, so it would also add another problem. The last solution studied here is to use structuration. It consists in implementing microstructures etched in the silicon layer. We can see different ways of improving photon-material interactions by the use of this kind of structures [2]. We count numerous structures that can have different impacts on the performances of a photodiode. There are nanowires [3]–[5], nanocones [6], [7], nanoholes [8]–[10], nanopillars [7], [8], [11], pyramids [12]–[16], paraboloid structures [17] and many others [18]–[23]. These

structures will help increase the absorption and therefore QE by two main phenomena. First, they will act as an antireflective layer, realizing a good matching between the incident material and the etched structures due to the gradual decrease of the effective index [7]. This will therefore limit reflection which is a big contributor of the lost signal in standard planar photodiodes. Secondly, they will diffract light inside the photodiode, resulting in an increase of the optical path inside the absorbing layer, and thus in an increase in absorption. Contrary to RCE, they are much more process compatible. Choosing pyramids, this structuration solution has been studied and some simulation and characterization results are presented. We can see other phenomena like Whispering Gallery modes [18], [21] that happen with some types of structure, but this will not be discussed further in this paper.

2. STUDIED STRUCTURES AND TOOLS

As mentioned before, we chose to study pyramids here. We can also realize trenches, with a dry etch process, but it was not of best interest in our case for the type of pixel that we have studied. Moreover, being realized by anisotropic wet etch, pyramid structures avoid having the Silicon surface exposed to plasma. An oxide layer is indeed first deposited on the Silicon, acting as a hard mask. We then pattern this hard mask by lithography, before etching the Silicon by wet chemistry that can be based on KOH for example. When applying it on a c-Si (111), it will indeed etch pyramids with a 54.7° angle between the (111) and (100) crystallographic planes. Then, the hard mask is removed by a selective wet etch using HF. Finally, antireflective layers are deposited on the silicon and an oxide is used for planarization. Two SEM images of a trench (Figure 1.a) and a pyramid (Figure 1.b) realized at STMicroelectronics are shown in Figure 1.

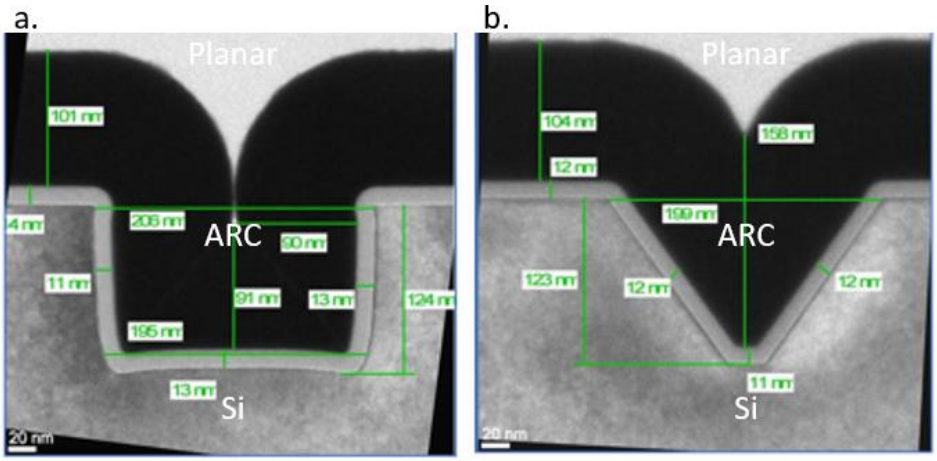

Figure 1. SEM images of a. a trench using dry etch process and b. a pyramid using wet etch process. The different layers are highlighted: Si (Silicon), ARC (Anti Reflective Coating) and Planar (Planarization layer)

These pyramids along with the entire pixel are fully reproduced in a Finite Difference Time Domain (FDTD) solver [24], in order to simulate the electromagnetic fields inside the pixel [25], [26]. This allow us to access numerous data like the one of interest here, which is the absorption in the Silicon layer. The parameter that we want to measure is the QE, which is equal to the ratio between the number of incoming photons over the number of collected electrons. Here, we did not perform a coupling between the optical and electrical simulations [27], so we cannot access the number of collected electrons but only the number of photogenerated ones, which is the absorption. In the next part, by convenience, we will only talk about QE even for simulation results, but the real simulated results are the absorptions.

These structures were then reproduced on Silicon, to perform some characterizations. First we did QE measurement to compare with simulated results. Our sensor is illuminated by a uniform diffuse light at 940nm with a ±7.5nm spectral dispersion. We indeed use an halogen source linked to a monochromator to obtain the wavelength of interest. It is then coupled into an integrating sphere to obtain a uniform illumination and we set a f/2 f-number as generally used. We recover the signal from all the different pixels of the sensor, to finally obtain the QE. We also did MTF measurements. As mentioned, when using these structures light will be diffracted enhancing the light path inside the photodiode. However this will also increase crosstalk. Some photons will indeed go through the Deep Trench Isolations (DTI)

separating two pixels and be absorbed in the wrong pixel. This will degrade our image. So, this is also an important parameter that needs to be considered. The MTF of the sensor will be degraded if the crosstalk increases. It indeed indicates how the modulation of a sinusoidal variation of intensity is reduced, depending on its spatial frequency. An illustration of a typical MTF curve is shown in Figure 2 along with the input pattern projected on the sensor and its output response according to the spatial frequency. Because these modulated patterns are not easy to produce with accuracy, we instead use the slanted edge method [28] to characterize the MTF of our sensors. It consists in projecting a black and white transition onto the sensor with a small angle (typically 5°) with respect to the vertical (respectively horizontal) direction of the sensor if the horizontal (respectively vertical) MTF is measured. Thanks to the tilt of the target transition we can recover the oversample response of the sensor called the oversampled Edge Spread Function (ESF). We then derive this function to obtain the Line Spread Function (LSF) and take the modulus of the Fourier transform of the LSF, which corresponds to the 1D projection of the MTF. To obtain the MTF of the sensor this computed MTF has to be divided by the MTF of the optics which is used to project the target on the characterization bench. We usually plot the MTF Corrected by a Perfect Optics (MTF CPO), which is a diffraction-limited optics free from aberrations, and the different MTF results presented in the next section correspond to these MTF CPO (worst case sensor MTF as corrected by a perfect optic MTF).

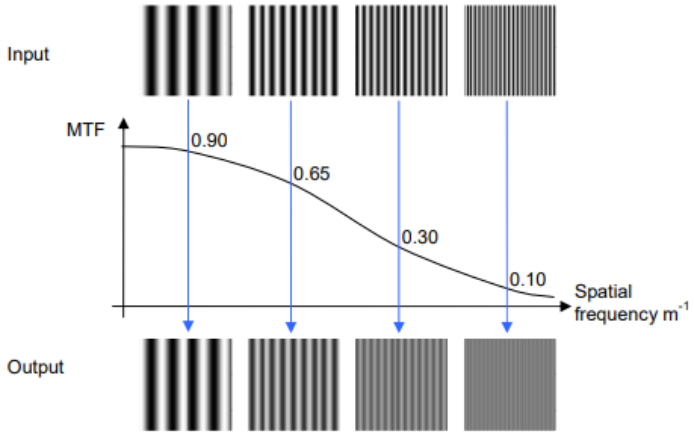

Figure 2. Illustration of a typical MTF curve showing the input modulation according to the spatial frequency and the output response of the sensor.

3. RESULTS

3.1 Quantum Efficiency

Two different Back Side Illuminated (BSI) pixels were investigated here: one with a 1.75µm pitch and one with a 3.2µm pitch. As Table 1 is showing, various pyramid arrays were tested on each pixel. For both, one trial is without pyramid, acting as a reference. Then, various configurations were tried: only one pyramid in the middle of the pixel (which is a square) called 1x1 pyramid configuration, an array of 2 by 2 similar pyramids also centered in the middle of the pixel (2x2 pyramids configuration), and for the biggest pixel, 3 by 3 and even 4 by 4 similar pyramids centered in the middle were also tested (3x3 and 4x4 pyramids configurations). The different parameters like the size of the pyramids, which corresponds to the base length of the right square pyramid that is formed, and the spacing between them if any are also presented in this table. By convenience, we call trials and versions the different pyramid tests on the 1.75µm and 3.2µm pixels respectively. We realized these different patterns using both a 3µm and a 6µm Silicon epitaxy (EPI) layer, to also compare the difference between a thin and a thicker photodiode. One can see the QE results of all the different versions and trials in Figure 3. and Figure 4. respectively. In Figure 3., there are two types of measurement: Package Level Characterization (PLC) and Wafer Level Characterization (WLC). The first one corresponds to the measurement of a single die that is extracted from the wafer, containing all the different pixel versions and is done at Room Temperature (RT). The second one is a measurement directly done on the wafer, on various dies and at 60°C.

Table 1. Definitions of the different trials and versions on the different pixels.

Pixel pitch (µm)	Trials and Versions	Configuration	Size (nm)	Spacing (nm)
1.75	T01	No pyramids: ref	NA	NA
	T02	1x1 pyramid	950	NA
	T03	2x2 pyramids	400	100
	T04	2x2 pyramids	520	100
3.2	V00	No pyramids: ref	NA	NA
	V01	1x1 pyramid	500	NA
	V02	1x1 pyramid	1000	NA
	V03	1x1 pyramid	1500	NA
	V04	1x1 pyramid	2000	NA
	V05	1x1 pyramid	2500	NA
	V06	2x2 pyramids	400	100
	V07	2x2 pyramids	900	100
	V08	2x2 pyramids	900	200
	V09	2x2 pyramids	900	300
	V10	3x3 pyramids	600	100
	V11	3x3 pyramids	600	200
	V12	3x3 pyramids	730	200
	V13	4x4 pyramids	570	100

It should be noted that this gap between the different temperatures explains why WLC results are higher than PLC ones. Finally, all the different simulations and measurements were done at 940nm with ±7.5nm Full Width Half Maximum (FWHM). It can be noticed that trends between simulations and characterizations are very similar. We can indeed see in Figure 3. c., d. and in Figure 4 c., d. that the gain, corresponding to the values of the different versions (or trials) over the reference V00 (or T01), is closed for every pattern between simulation and characterization (even if correlation is better for the 3.2µm pixel). However, simulation results are overestimated the real QE seen in characterization: there are always higher than the measured values (see Figure 3. a., b. and Figure 4. a., b.). As mentioned in the previous section, since we did not realize electrical simulations but only optical ones, the simulated QE that is shown is in fact the absorption but not all the absorbed signals will be transmitted and read, hence this overestimation. Nevertheless, no matter the configuration, we always see a QE gain which can be huge: it is up to 2.4 for the PLC characterizations on the 3.2µm pixel with a 3µm thick EPI (Figure 3. c.). The maximum QE is obtained for V03 which corresponds to a 1500nm wide single pyramid and reaches 47% at RT (PLC) and 55% at 60°C (WLC). More generally, it seems that the single pyramid array gives the best QE results after having a certain size (more than 1000nm). V02 to V04 are indeed giving higher QE values than all the other versions. As for V05, there was a problem processing such a big pyramid, this is why we only have simulated results. But according to the simulation, it would have also been an important value. Concerning the 1.75µm pixel, T02 and T04 give more or less the same results, but for T02 the pyramid was smaller than 1000nm, we can therefore do the assumption that we would have seen better results with a 1500nm wide pyramid, but it was not possible on this small pixel, taking into account the size of the DTI. For all the other configurations, we obtain similar results.

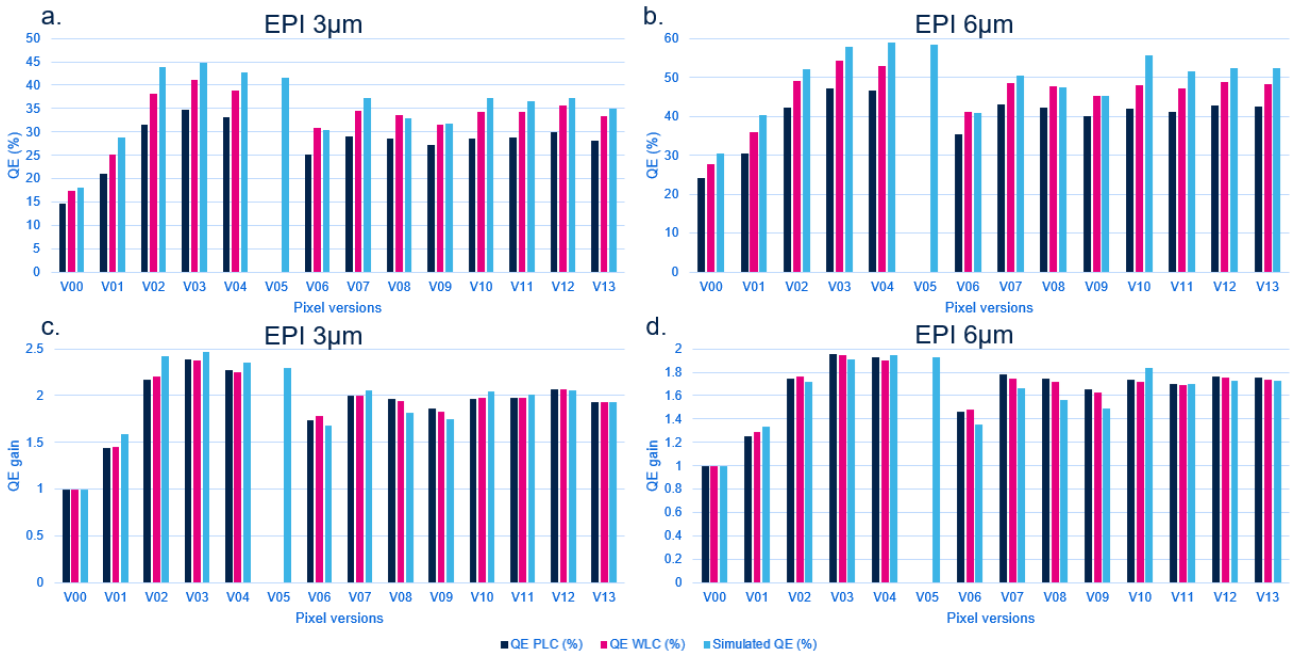

Figure 3. QE measurement and simulation results of the 3.2µm pixel at 940nm for the different pixel versions for a. a 3µm thick Silicon epitaxy and b. a 6µm thick Silicon epitaxy. QE gain of the 3.2µm pixel at 940nm measured and simulated with respect to the reference version (V00) for c. a 3µm thick Silicon epitaxy and d. a 6µm thick Silicon epitaxy. There are Two types of measurement: Package Level Characterization (PLC) and Wafer Level Characterization (WLC) which correspond respectively to measurements on a single die or on an entire wafer. PLC measurement were done at RT whereas WLC measurements were characterized at 60°C.

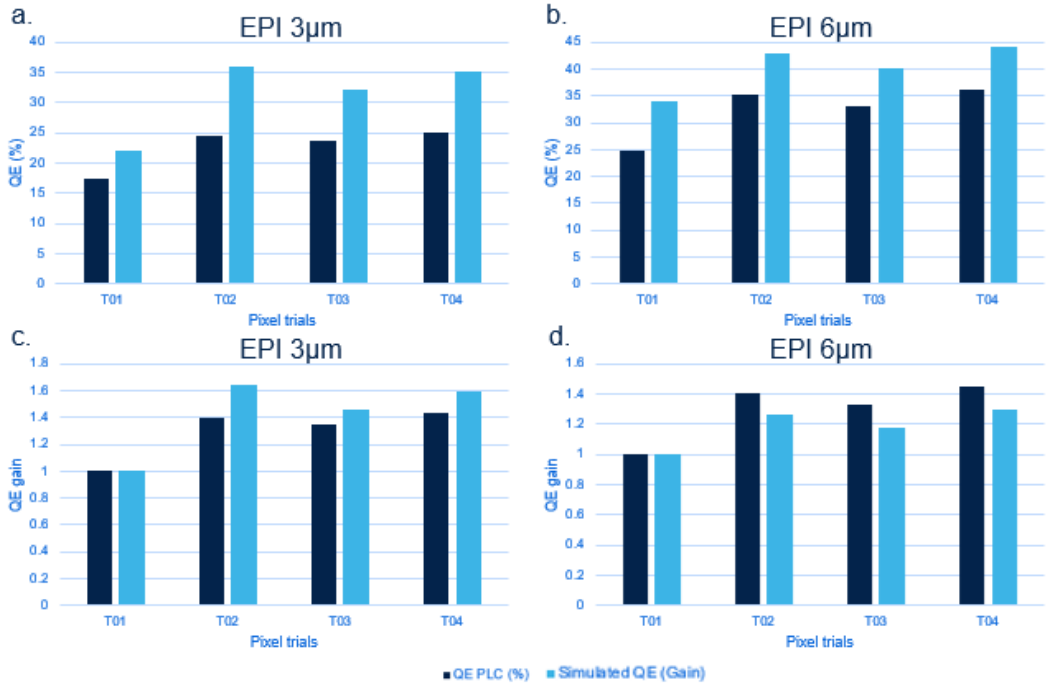

Figure 4. QE measurement and simulation results of the 1.75µm pixel at 940nm for the different pixel trials for a. a 3µm thick Silicon epitaxy and b. a 6µm thick Silicon epitaxy. QE gain of the 1.75µm pixel at 940nm measured and simulated with respect to the reference trial (T01) for c. a 3µm thick Silicon epitaxy and d. a 6µm thick Silicon epitaxy.

Finally, an important gain is observed for all the different versions and trials as we increase the EPI. By doing so, we indeed increase the absorption volume of our photodiode. It therefore seems logical that we are improving QE. An interesting result to notice is that the trends between the 3µm and 6µm EPI pixels are the same: the differences between one version to the other are approximately the same. However, the gain is smaller for the 6µm EPI case. It means that the reference pixel (V00 or T01) is more impacted by this increase in the EPI thickness than the structured ones are.

3.2 Modulation Transfer Function

Figure 5. is showing the different MTF results at Nyquist (Ny) and Ny/2 spatial frequencies, which are the common values of interest for this parameter. First, we can see that the trends between horizontal and vertical MTF are nearly the same for the four different graphs. An exception is pointed out in Figure 5. b. for V03 and V04, where the horizontal MTF at Ny/2 is much higher than the vertical one. Moreover, we can see a little difference between the horizontal and vertical MTF. This is linked to the pixel's architectures and not on the structuration patterns, because in this study, there were totally symmetric. We can indeed note that this difference is maintained between the different versions or trials. Secondly, as expected, V00 and T01 have respectively the best MTF. As previously mentioned, when adding diffractive structures, crosstalk is increased and therefore MTF is degraded. We can also see a MTF improvement when we increase the EPI. A greater portion of light is absorbed in the corresponding pixel: it leaks less in the neighboring pixels. Finally, one can notice that the versions with the lowest MTF correspond to the versions with the highest QE previously seen. This will be the topic of the next section.

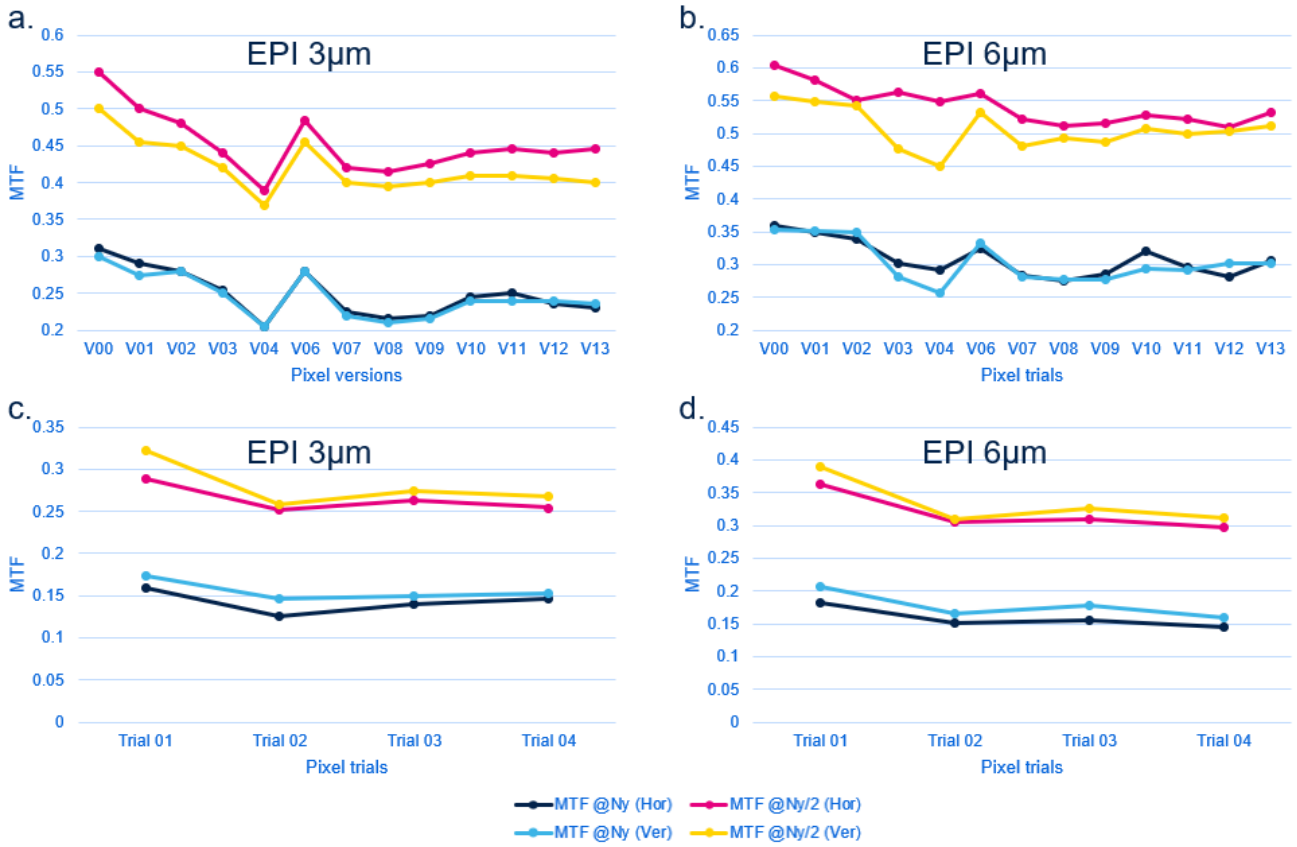

Figure 5. Horizontal and vertical MTF at Ny and Ny/2 for a. the different versions of the 3.2µm pixel with a 3µm EPI, b. the different versions of the 3.2µm pixel with a 6µm EPI, c. the different trials of the 1.75µm pixel with a 3µm EPI, d. the different trials of the 1.75µm pixel with a 6µm EPI.

3.3 Comparison between measured data: Quantum Efficiency vs Modulation Transfer function

Figure 6. is representing the different QE with respect to the horizontal MTF at Ny/2 (knowing that the vertical MTF have the same trends). In both pixel cases, QE and MTF are improved when we go from a 3µm to a 6µm EPI. Increasing furthermore this parameter would be benefic for both QE and MTF. But it would come with process and rapidity issues for applications where a small electron transit time is needed. Moreover, as briefly mentioned above, increasing QE is generally decreasing the MTF. But for versions with approximately the same QE, we can find a configuration that maximizes the MTF. For example, as we can see in Figure 6., for the 6µm EPI case V02 has the same QE than V07 to V13 but has a much better MTF at Ny/2. It is even more pronounced in the 3µm case, where not only its MTF is better, but also its QE. It therefore seems that not only single pyramid arrays are obtaining the best QE performances, but they also maximize MTF. We do not see such results for the 1.75µm pixel in the 6µm EPI case but this is mainly due to a lack of trials for this pixel. For the 3.2µm pixel, we clearly see a trend for the single pyramid array: the more the size is increased the better is the QE but the more degraded is the MTF. It works up to a 1500nm pyramid, and above this limit QE is no longer increased but MTF is still degraded (V03 compared to V04). For the other pyramid configurations, except for V06 and probably linked to the small size of its pyramids, QE and MTF are very similar and contained in the same area of the graph. Finally, the choice of the different type of structuration is a trade-off between QE and MTF. Nevertheless, with respect to the reference without any structuration, we can find designs with a significative QE gain without degrading a lot the MTF.

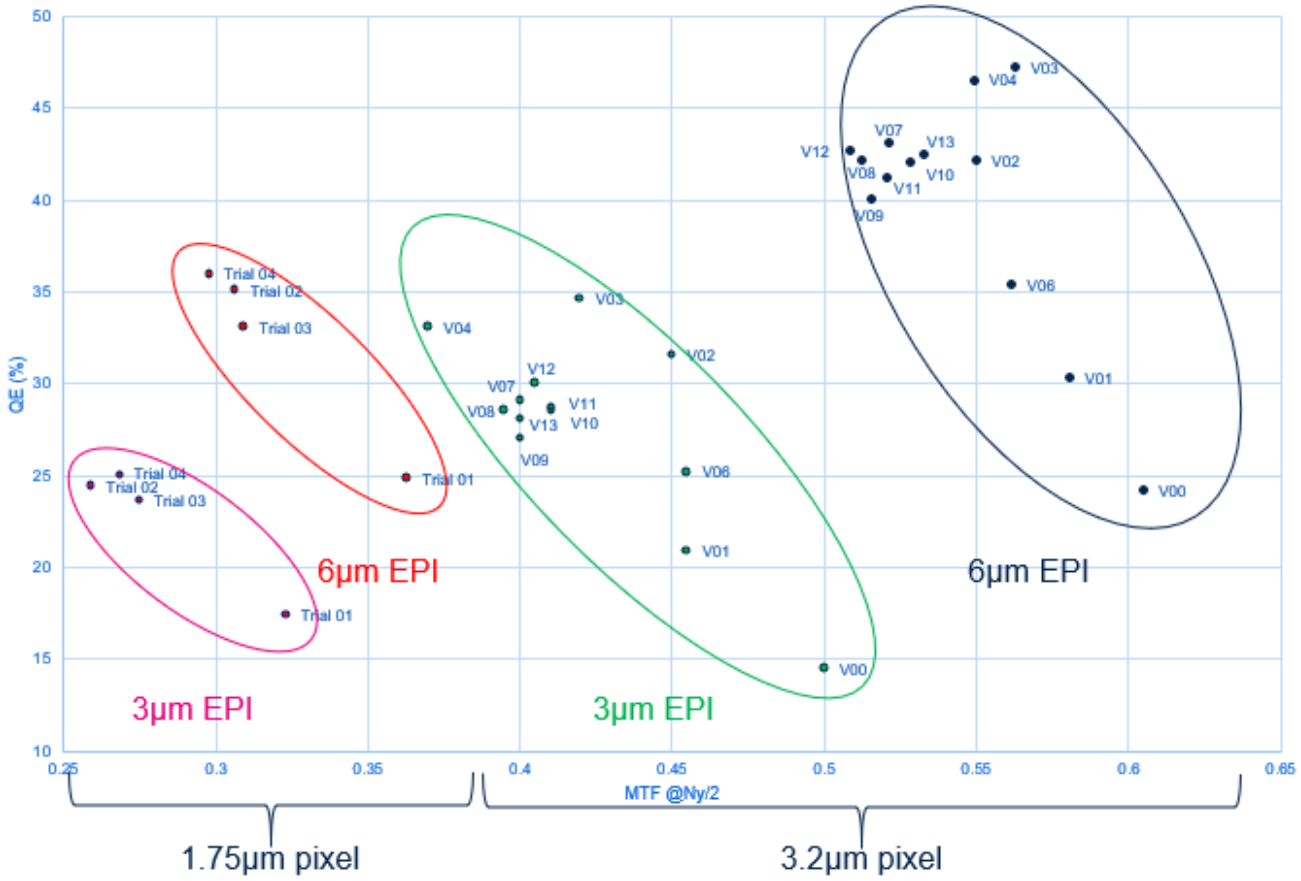

Figure 6. Characterization graph of QE vs Horizontal MTF at Ny/2 for the different pixel trials and versions.

4. CONCLUSION

This study has shown very promising results concerning the improvement of CMOS image sensor optical performances in the NIR. We indeed observe great QE gains for single pyramid arrays with a degraded but still high MTF. Simulation predictions were confirmed by characterization, which will be the key to enable an optimization on the different patterns and configurations to find the best trade-off between QE and crosstalk. We can indeed think of other structures to enhance QE. For example, we can use rectangular trenches (dry etch process) in order to diffract light in a specific direction and avoid some critical regions (like memories). The MTF in that direction will be degraded but some parasitic light could be decreased at the same time. We can also use structures to have a different excitation between light and matter, for example we could excite whispering gallery modes [18]. Moreover, random structures with the use of an optimization algorithm could also be a way to improve both QE and MTF at the same time. This will be part of a future study. Finally, metal could be implemented inside the DTI in order to increase the isolation between pixels and therefore reduce crosstalk while keeping a high QE. To conclude, all these different techniques could contribute to improve further the optical performances of CMOS image sensors in the NIR.

REFERENCES

[1] M. S. Ünlü, M. K. Emsley, O. I. Dosunmu, P. Muller, and Y. Leblebici, "High-speed Si resonant cavity enhanced photodetectors and arrays," *J. Vac. Sci. Technol. Vac. Surf. Films*, vol. 22, no. 3, p. 781, 2004, doi: 10.1116/1.1647591.

[2] H. Cansizoglu *et al.*, "A New Paradigm in High-Speed and High-Efficiency Silicon Photodiodes for Communication—Part I: Enhancing Photon–Material Interactions via Low-Dimensional Structures," *IEEE Trans. Electron Devices*, vol. 65, no. 2, pp. 372–381, Feb. 2018, doi: 10.1109/TED.2017.2779145.

[3] E. Garnett and P. Yang, "Light Trapping in Silicon Nanowire Solar Cells," *Nano Lett.*, vol. 10, no. 3, pp. 1082–1087, Mar. 2010, doi: 10.1021/nl100161z.

[4] D. R. Kim, C. H. Lee, P. M. Rao, I. S. Cho, and X. Zheng, "Hybrid Si Microwire and Planar Solar Cells: Passivation and Characterization," *Nano Lett.*, vol. 11, no. 7, pp. 2704–2708, Jul. 2011, doi: 10.1021/nl2009636.

[5] T. J. Kempa *et al.*, "Coaxial multishell nanowires with high-quality electronic interfaces and tunable optical cavities for ultrathin photovoltaics," *Proc. Natl. Acad. Sci.*, vol. 109, no. 5, pp. 1407–1412, Jan. 2012, doi: 10.1073/pnas.1120415109.

[6] S. Jeong, M. D. McGehee, and Y. Cui, "All-back-contact ultra-thin silicon nanocone solar cells with 13.7% power conversion efficiency," *Nat. Commun.*, vol. 4, no. 1, p. 2950, Dec. 2013, doi: 10.1038/ncomms3950.

[7] H. Lin *et al.*, "Developing controllable anisotropic wet etching to achieve silicon nanorods, nanopencils and nanocones for efficient photon trapping," *J. Mater. Chem. A*, vol. 1, no. 34, p. 9942, 2013, doi: 10.1039/c3ta11889d.

[8] Y. Gao *et al.*, "Photon-trapping microstructures enable high-speed high-efficiency silicon photodiodes," *Nat. Photonics*, vol. 11, no. 5, pp. 301–308, May 2017, doi: 10.1038/nphoton.2017.37.

[9] S.-F. Leung *et al.*, "Efficient Photon Capturing with Ordered Three-Dimensional Nanowell Arrays," *Nano Lett.*, vol. 12, no. 7, pp. 3682–3689, Jul. 2012, doi: 10.1021/nl3014567.

[10] J. L. Donnelly *et al.*, "Mode-based analysis of silicon nanohole arrays for photovoltaic applications," *Opt. Express*, vol. 22, no. S5, p. A1343, Aug. 2014, doi: 10.1364/OE.22.0A1343.

[11] P. Spinelli, M. A. Verschuuren, and A. Polman, "Broadband omnidirectional antireflection coating based on subwavelength surface Mie resonators," *Nat. Commun.*, vol. 3, no. 1, p. 692, Jan. 2012, doi: 10.1038/ncomms1691.

[12] M. S. Branham *et al.*, "15.7% Efficient 10-μm-Thick Crystalline Silicon Solar Cells Using Periodic Nanostructures," *Adv. Mater.*, vol. 27, no. 13, pp. 2182–2188, Apr. 2015, doi: 10.1002/adma.201405511.

[13] S. E. Han and G. Chen, "Toward the Lambertian Limit of Light Trapping in Thin Nanostructured Silicon Solar Cells," *Nano Lett.*, vol. 10, no. 11, pp. 4692–4696, Nov. 2010, doi: 10.1021/nl1029804.

[14] I. Oshiyama *et al.*, "Near-infrared sensitivity enhancement of a back-illuminated complementary metal oxide semiconductor image sensor with a pyramid surface for diffraction structure," in *2017 IEEE International Electron Devices Meeting (IEDM)*, San Francisco, CA, USA, Dec. 2017, p. 16.4.1-16.4.4. doi: 10.1109/IEDM.2017.8268403.

[15] S. Yokogawa *et al.*, "IR sensitivity enhancement of CMOS Image Sensor with diffractive light trapping pixels," *Sci. Rep.*, vol. 7, no. 1, p. 3832, Dec. 2017, doi: 10.1038/s41598-017-04200-y.

[16] K. Zang *et al.*, "Silicon single-photon avalanche diodes with nano-structured light trapping," *Nat. Commun.*, vol. 8, no. 1, p. 628, Dec. 2017, doi: 10.1038/s41467-017-00733-y.

[17] F. Khan, S.-H. Baek, J. Kaur, I. Fareed, A. Mobin, and J. H. Kim, "Paraboloid Structured Silicon Surface for Enhanced Light Absorption: Experimental and Simulative Investigations," *Nanoscale Res. Lett.*, vol. 10, no. 1, p. 376, Dec. 2015, doi: 10.1186/s11671-015-1087-9.

[18] K. Kim *et al.*, "Whispering gallery modes enhance the near-infrared photoresponse of hourglass-shaped silicon nanowire photodiodes," *Nat. Electron.*, vol. 2, no. 12, pp. 572–579, Dec. 2019, doi: 10.1038/s41928-019-0317-z.

[19] S. S. P. Konedana, E. Vaida, V. Viller, and G. Shalev, "Optical absorption beyond the Yablonovitch limit with light funnel arrays," *Nano Energy*, vol. 59, pp. 321–326, May 2019, doi: 10.1016/j.nanoen.2019.02.039.

[20] S.-F. Leung *et al.*, "Light Management with Nanostructures for Optoelectronic Devices," *J. Phys. Chem. Lett.*, vol. 5, no. 8, pp. 1479–1495, Apr. 2014, doi: 10.1021/jz500306f.

[21] Y. Yao *et al.*, "Broadband light management using low-Q whispering gallery modes in spherical nanoshells," *Nat. Commun.*, vol. 3, no. 1, p. 664, Jan. 2012, doi: 10.1038/ncomms1664.

[22] K. J. Yu *et al.*, "Light Trapping in Ultrathin Monocrystalline Silicon Solar Cells," *Adv. Energy Mater.*, vol. 3, no. 11, pp. 1401–1406, Nov. 2013, doi: 10.1002/aenm.201300542.

[23] J. Zhu, C.-M. Hsu, Z. Yu, S. Fan, and Y. Cui, "Nanodome Solar Cells with Efficient Light Management and Self-Cleaning," *Nano Lett.*, vol. 10, no. 6, pp. 1979–1984, Jun. 2010, doi: 10.1021/nl9034237.

[24] <*https://www.lumerical.com/*>

[25] J. Vaillant, A. Crocherie, F. Hirigoyen, A. Cadien, and J. Pond, “Uniform illumination and rigorous electromagnetic simulations applied to CMOS image sensors,” p. 10, 2007.
[26] G. Chataignier and B. Vandame, “Joint electromagnetic and ray-tracing simulations for quad-pixel sensor and computational imaging,” p. 16.
[27] “IISW09_From_photons_to_electrons_a_complete_3D_simulation_flow_for_CMOS_Image_Sensor,” p. 4, 2009.
[28] P. Burns, “Slanted-Edge MTF for Digital Camera and Scanner Analysis,” p. 4.